

## Technical Note

# An Intermetallic NiTi-Based Shape Memory Coil Spring for Actuator Technologies

Ganesh Shimoga <sup>\*</sup>, Tae-Hoon Kim  and Sang-Youn Kim <sup>\*</sup>

Interaction Laboratory, Future Convergence Engineering, Advanced Technology Research Center, Korea University of Technology and Education, Cheonan-si 31253, Chungcheongnam-do, Korea; taehoon@koreatech.ac.kr

\* Correspondence: shimoga@koreatech.ac.kr (G.S.); sykim@koreatech.ac.kr (S.-Y.K.); Tel.: +82-041-560-1484 (S.-Y.K.)

**Abstract:** Amongst various intermetallic shape memory alloys (SMAs), nickel–titanium-based SMAs (NiTi) are known for their unique elastocaloric property. This widely used shape remembering material demonstrates excellent mechanical and electrical properties with superior corrosion resistance and super-long fatigue life. The straight-drawn wire form of NiTi has a maximum restorable strain limit of ~4%. However, a maximum linear strain of ~20% can be attained in its coil spring structure. Various material/mechanical engineers have widely exploited this superior mechanic characteristic and stress-triggered heating/cooling efficiency of NiTi to design smart engineering structures, especially in actuator technologies. This short technical note reflects the characteristics of the NiTi coil spring structure with its phase transformations and thermal transformation properties. The micro-actuators based on NiTi have been found to be possible, suggesting uses from biomedical to advanced high-tech applications. In recent years, the technical advancements in modular robotic systems involving NiTi-based SMAs have gained speculative commercial interest.



**Citation:** Shimoga, G.; Kim, T.-H.; Kim, S.-Y. An Intermetallic NiTi-Based Shape Memory Coil Spring for Actuator Technologies. *Metals* **2021**, *11*, 1212. <https://doi.org/10.3390/met11081212>

Academic Editors: Maciej Motyka and João Pedro Oliveira

Received: 11 June 2021  
Accepted: 27 July 2021  
Published: 29 July 2021

**Publisher's Note:** MDPI stays neutral with regard to jurisdictional claims in published maps and institutional affiliations.



**Copyright:** © 2021 by the authors. Licensee MDPI, Basel, Switzerland. This article is an open access article distributed under the terms and conditions of the Creative Commons Attribution (CC BY) license (<https://creativecommons.org/licenses/by/4.0/>).

## 1. Introduction

Tetsuro Mori, an eminent senior engineer of Yaskawa Electric Corporation, in 1969, coined the word “mechatronics”. Technically speaking, mechatronics is an interdisciplinary branch of intensive engineering, which involves the unification of electronic and mechanical systems, with interlinking aspects of computer system engineering and control system engineering (see Figure 1). The best example of a mechatronic system is an industrial robot, which operates at the intersection of electronics, mechanics, and computing to perform its routine tasks [1–4]. In the past few decades, the advancement in mechatronics has implicated its use from biomedical fields to the technology arena [5,6].

Electromechanical actuators and electromagnetic sensors are the two most imperative components of mechatronic systems. Designing various electromechanical and electromagnetic device modules is crucial in the automotive and robotic industries. Utilization of the material properties and material selection criteria plays an important role in constructing electromechanical actuator modules [7,8]. Shape memory alloys (SMAs) are broadly used in the development of thermostatic and electromechanical actuators, to perform mechanical actions assisted by temperature change phenomena via electric currents. To improve the robustness, the compact and straightforward design strategy was usually adopted [9–11]. Amongst various type of SMAs, nickel–titanium (NiTi)-based SMAs (commonly known as NiTi) are preferably used in most smart engineering structures and actuator technologies due to their exceptional thermo-mechanical performances, practicability, shape memory characteristics, and pseudoelasticity [12–15].

The thermal shape memory effect of SMAs during the actuation cycle involves two stable phases, namely austenite and martensite. Under the influence of temperature and

stress, three dissimilar crystal structures (viz. twinned martensite, detwinned martensite, and austenite) are possible with transformation in the atomic arrangements (see Figure 2). Due to alteration in the microstructural array arrangement during phase transition, the discrepancy in the mechanical properties (yield strength and Young's modulus) can be noticed [16–19]. In particular, NiTi can be deformed in its martensite phase and, upon heating, it can return to its original shape. Briefly, the austenite phase is cooled down to the twinned martensite phase. This martensite phase can be deformed by applied external stress. Then, when thermally stimulated, the material returns to its original shape. This anomaly can be referred as the “shape memory effect” [20]. NiTi exhibits Lüders-like deformation under a variety of testing conditions and, for easy understanding, three testing environments are provided here: (I) the tensile distortion related to the stress-induced martensitic transformation from the austenite phase, (II) the reverse transformation of the stress-induced martensite to austenite in “pseudoelasticity”, and (III) the deformation in the martensitic state via a martensite variant reorientation process [21]. A stress plateau and a stress drop at the beginning of the process for the forward transformation upon loading and a stress minimum for the reverse transformation on unloading characterize the Lüders-like deformation behavior [21,22]. As we know, Schmid's law describes the slip plane and the slip direction of a stressed material well, and the martensite transformation shows good agreement with Schmid's law [23]. Indeed, martensite transformations are unique due to their reversible characteristics and self-accommodating nature of martensite plates [24].

NiTi can withstand large deformations, that is, austenite can, under high stress, transform into stress-induced martensite. Since SMAs are unidirectional actuators, external stress must be applied to strain it to its detwinned state, and to relapse its highly organized (austenite) crystal structure, thermal acceleration is essential [19]. Despite electroactive polymers and piezoelectric materials, NiTi SMAs can develop high stresses (~560 MPa in austenitic phase and ~100 MPa in martensitic phase) in wires of ~0.5 mm in thickness [25].

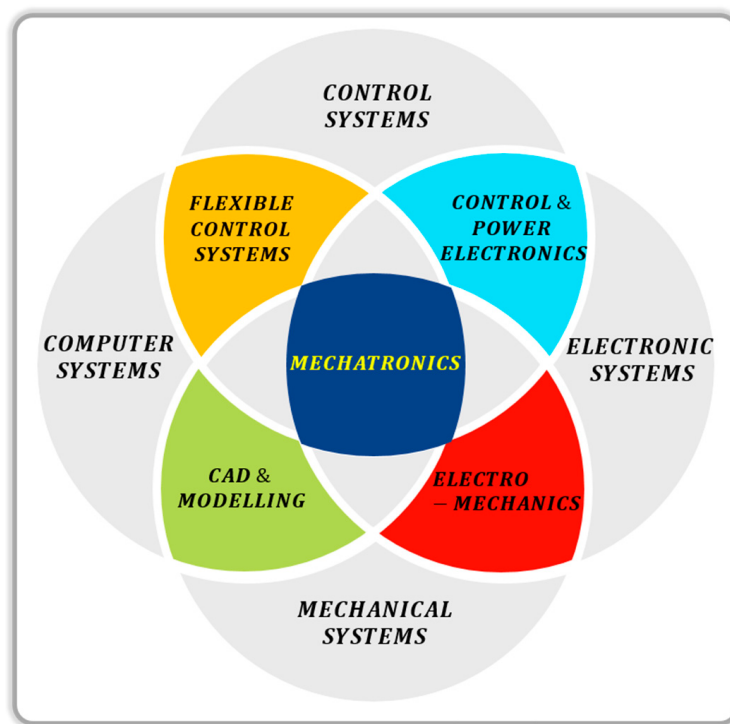


**Figure 1.** Euler diagram representation of mechatronics and its interdisciplinary branches of engineering.

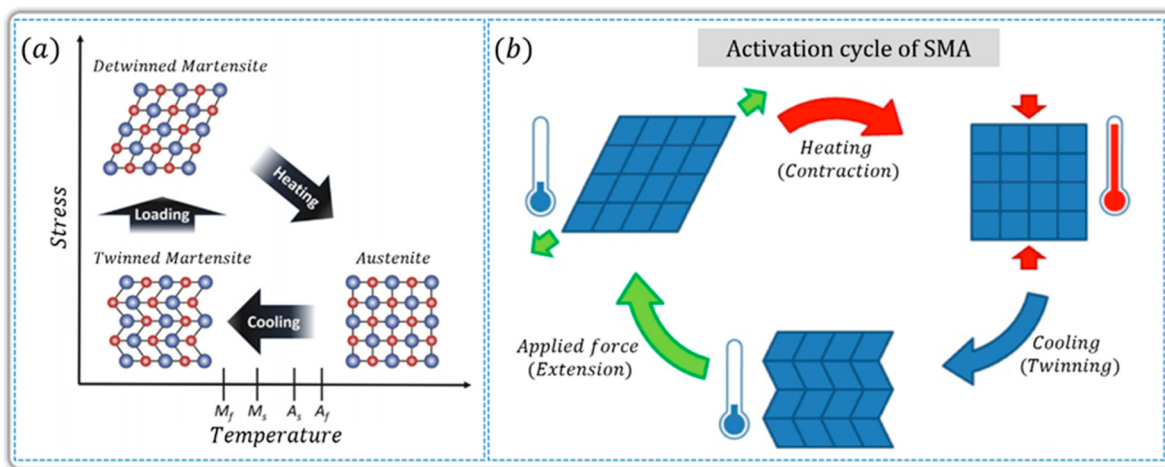


**Figure 2.** (a) Phase transition behavior of SMAs, adapted with permission from [18], Elsevier, 2016. (b) Activation cycle of SMAs under the influence of temperature, adapted with permission from [19], IEEE, 2014. (Note:  $A_f$  = Austenite finish temperature,  $A_s$  = Austenite start temperature,  $M_s$  = Martensite start temperature, and  $M_f$  = Martensite finish temperature).

Divergent applications of NiTi have been developed for actuator technologies, especially in robotic science and engineering [26]. The widespread use of NiTi is due to its fatigue behavior and sturdiness. Depending on the customized applications, NiTi is commercially available in various forms (see Figure 3). The corrosion resistance and biocompatibility of NiTi caused it to gain immense interest for biomedical applications by allowing it to be used in invasive surgical instruments and medical implants [27].

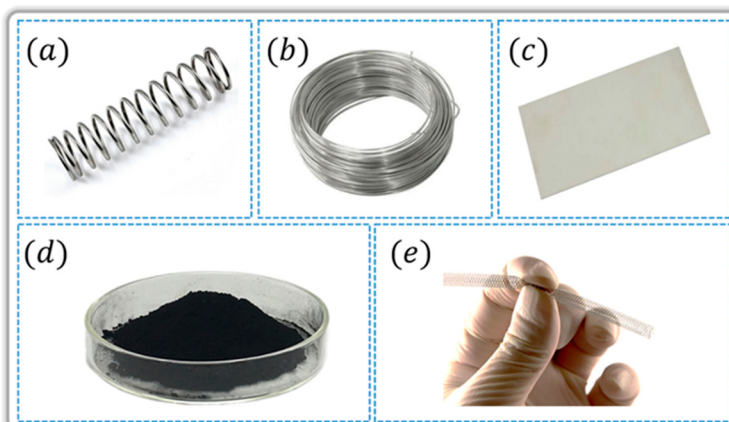


**Figure 3.** Various forms of commercially available NiTi: (a) spring, (b) wire, (c) thin film, (d) nanoparticles, (e) stent (demonstrating squeezing of a self-expanding braided NiTi stent used for endovascular surgery) [12].

There are three operational phases in NiTi, namely (I) an austenitic phase, (II) a martensitic phase, and (III) an intermediate R-phase. A well-ordered and highly symmetric body-centered cubic (BCC) crystal lattice structure denoted as a B2 structure was encountered in the austenitic phase, resembling cesium chloride (cubic crystal lattice structure), in which body-centered and corner atoms do not have similar neighborhood atoms [28,29]. In the case of the martensitic phase, a complex twinned B19' (monoclinic) crystal structure can be observed with low symmetry, stabilized by residual stresses (see Figure 4). The arrangement of atoms in the martensitic phase can be compared to herringbone-patterned needle-like crystal arrays. The martensite is more ductile with a softer entity [30]. Compared to the martensitic phase, the austenitic phase is harder and more rigid. In some NiTi grades, primarily when additionally alloyed with a ferrous element, an inter-

mediate R-phase can be encountered with a rhombohedral crystal structure displaying low-temperature hysteresis (1–10 °C) and low transformation strain [31–33].

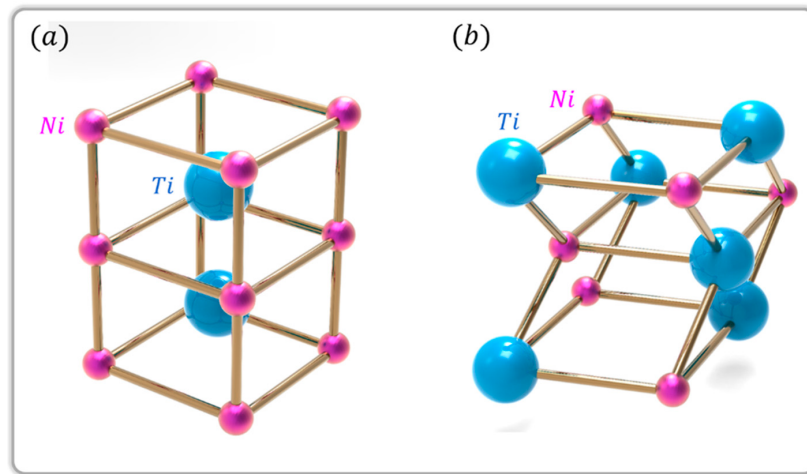


**Figure 4.** Crystal structure phases of NiTi displaying (a) B2 austenitic phase, and (b) B19' martensitic phase (Designed by T.-H.K.).

Superelasticity is the characteristic property which is displayed by NiTi-based SMA wires. The superelasticity refers to the reversible transformation of the martensitic phase, which is triggered due to the variation in stress state. As we can see from Figure 5, an adequate tensile load activates the transformation of phases from austenite into detwinned martensite. While unloading, the stress-induced martensitic phase reverts to the austenitic phase via a partially detwinned martensitic phase. In general, the stress-induced martensitic phase is one of the martensitic phases, which forms from austenite in the existence of stress. There are many thermomechanical loading paths that can result in the formation of stress-induced martensitic phases. In general, both the ‘superelastic’ and ‘rubber-like’ behaviors are labeled as ‘pseudoelasticity’. The reversible phase transformation caused by a thermomechanical loading path is called the superelastic behavior [34,35]. The rubber-like effect is an exclusive behavior of the martensite phase and occurs due to the reversible reorientation of martensite (the martensite crystals may be more pliable, equally stiff, or stiffer than austenite crystals, depending on the orientation of the loading direction with respect to the unit cells) [36].

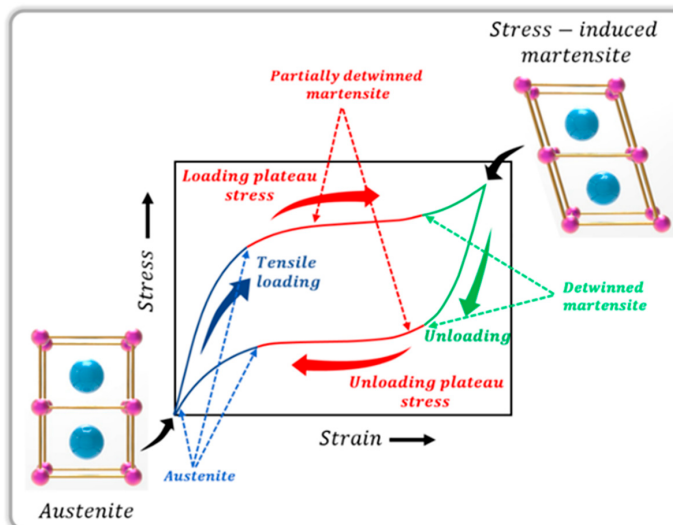


**Figure 5.** Typical stress–strain curve for the superelasticity of NiTi-based SMAs (Designed by T.-H.K. and G.S.).

## 2. Characteristics of NiTi Coils

In recent years, various mechatronic system module and robotic system studies have focused on utilizing NiTi-based materials as actuators. This proliferation of research activities in actuator technologies involving NiTi-based materials, especially wire and/or spring units to construct linear and rotary actuators, has been consistently documented [37–40]. The typical straight-drawn wire form of commercial NiTi has a maximum restorable strain limit of ~4%. A preeminent strain can be achieved by coiling the wire to resolve the applied force for increased strain. A maximum linear strain of ~20% can be achieved using coiled NiTi wires by successively tuning its shape memory properties in the linear coil model [41–43]. An example of a NiTi coil is schematically represented in Figure 6.

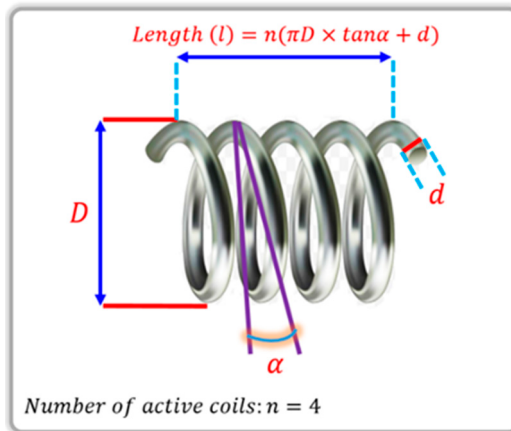


**Figure 6.** Geometrical design of a NiTi coil spring, representing thickness ( $d$ ), outer diameter ( $D$ ), length ( $l$ ), number of turns in the coil ( $n$ ), and initial pitch angle ( $\alpha$ ); (Designed by G.S.).

Depending on the crystal phases, we can notice two different shear moduli,  $G_A$  and  $G_M$ , respectively, for complete austenitic and martensitic crystal phases. The effective spring constant ( $K$ ) can be expressed by the following Equation (1) and is a function of the shear modulus ( $G$ ) of the respective NiTi phases; therefore, it is obvious that tuning of the stiffness and contractile properties can be possible by changing ' $d$ ', ' $D$ ', and ' $n$ ' [43].

$$K = \frac{Gd^4}{8nD^3} \quad (1)$$

Considering the actuation cycle of a NiTi spring, it generally commences from the martensite phase with an external load of  $F$ . Later, the spring is stimulated by inducing a suitable temperature until the transition temperature, resulting in the contraction of spring length under the applied load. The effective displacement ( $\delta_{eff}$ ) created by this phenomenon can be determined by Equation (2) (please refer Figure 7 for better understanding of indexes  $H$ ,  $L$ , and  $M$ ).

$$\delta_{eff} = \delta_M + \delta_L - \delta_H \quad (2)$$

With the displacement of the coil  $\delta_i$  under applied load  $F$ , where  $i \in \{H, L, M\}$ , using the general coiled spring deflection equation, Equation (1) can be written as Equation (3):

$$\delta_i = \frac{8FnD^3}{Gd^4}. \quad (3)$$

The shear strain  $\gamma$  of the spring can be written as

$$\gamma = \frac{\tau}{G} \quad (4)$$

where shear stress  $\tau$  can be expressed as

$$\tau = \frac{8FD\kappa}{\pi d^3}. \quad (5)$$

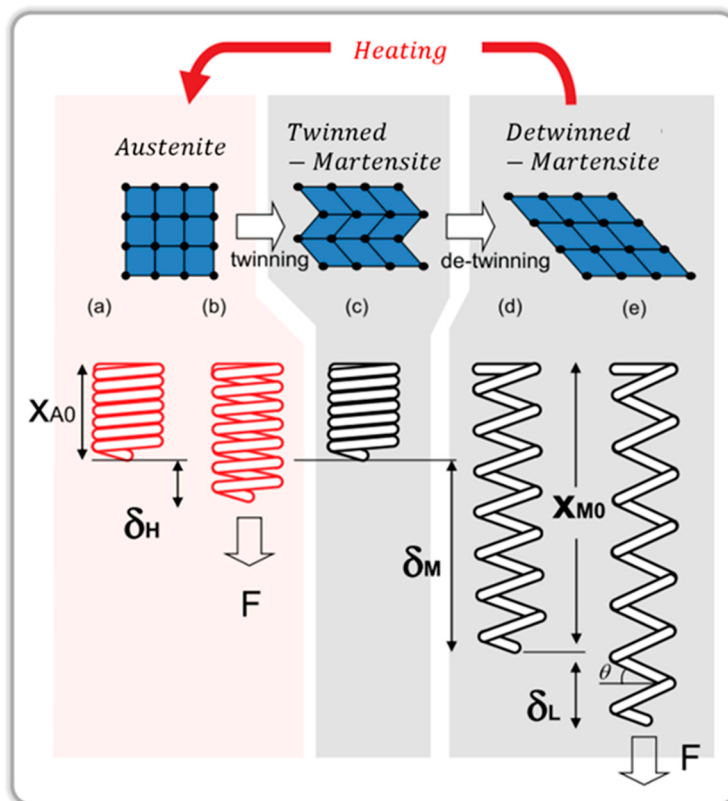


**Figure 7.** Five characteristic representative states of NiTi coil spring actuator. (a) Complete austenite phase without load, (b) complete austenite phase with load, (c) twinned martensite phase without load, (d) complete detwinned martensite phase without load, and (e) complete detwinned martensite phase with load. Adapted with permission from [43], IEEE, 2013.

From Wahl's formula [44], the stress correction factor  $\kappa$  can be written as

$$\kappa = \frac{4C - 1}{4C - 4} + \frac{0.615}{C} \quad (6)$$

where  $C$  is the spring index, and is defined as follows

$$C = \frac{D}{d}. \quad (7)$$

From Equations (3)–(5), the free length difference between the austenitic phase and martensitic phase can be calculated as follows:

$$\delta_M = \frac{\pi\gamma n D^2}{d\kappa}. \quad (8)$$

Consequently, the effective displacement from Equation (2) can be written as follows:

$$\delta_{eff} = \frac{\pi\gamma n D^2}{d\kappa} + \frac{8FnD_{eff}^3}{G_M d^4} - \frac{8FnD^3}{G_A d^4}. \quad (9)$$

The effective change in coil diameter of the spring ( $D_{eff}$ ), due to the elongation under the applied load  $F$  in the martensite phase, can be written as below, where  $\theta$  is the angle between the horizontal plane and the spring string (see Figure 7e).

$$D_{eff} = D \cos \theta \quad (10)$$

Figure 7 clearly demonstrates the actuation characteristics of a NiTi coil spring under different states. Under the thermal stimulation, when the temperature is applied to the NiTi spring, due to the contraction phenomenon, it converts to the austenitic phase (as shown in Figure 7a). The spring will have a displacement  $\delta_H$  when a load  $F$  is applied in this state (see Figure 7b). No noticeable shape change can be observed, beyond the transition temperature and the phase conversion from martensitic phase to austenitic phase can be seen (see Figure 7c). The detwinning of the crystal structure can be seen if the load is affixed below the transition temperature. Figure 7e,d, respectively, represent the detwinned martensitic phase with a load  $F$  and detwinned martensitic phase as its free length after removing the detwinning load. The free length difference between the austenite and detwinned martensite phases is denoted by  $\delta_M$ , where  $\delta_L$  signifies the length difference between the loaded and unloaded martensitic phase under complete detwinned mode [45,46].

### 3. Characteristic Properties and Features of NiTi

As mentioned earlier, the drawbacks of SMA wires are limited stroke and the prerequisite of high recovery force. This can be minimized by shaping them into a spring structure. The developed actuators made of coiled spring structures can withstand the maximum force and stroke. Another peculiar advantage of SMAs is that they can work effortlessly in liquid surroundings without effectively losing their mechanical properties [47]. The key advantage is the propulsion mechanism of bioinspired robots that can be constructed logically using SMAs, which can work favorably in both air and underwater environments. With increasing propensity to develop lightweight and tiny actuators with a high power/weight ratio, the actuators made of SMAs show compelling advantages over the conventional hydraulic, pneumatic, and electric actuators, as a convincing substitute for conventional technologies [47–50]. The high work density ( $10^4$ – $10^5$  KJ m<sup>-3</sup>), high force to weight ratio (~100), and quick actuation response (<1 s) of SMAs have inspired scientists to construct bioinspired soft actuation modules [51]. The SMAs suffer from a relatively lower actuation bandwidth (0.5–5 Hz) and energy efficiency of ~3% [52]; this is because of passive cooling at the terminal of the respective actuation cycles and wasting of energy due to heat loss in both cooling and activation cycles. To minimize these effects, SMA wires can be embedded inside various thermally conductive elastomeric materials while constructing soft robotic modules for morphing aircraft designs [53].

The metallic composition of nickel and titanium plays a crucial role in deciding the shape memory characteristics of NiTi. Normally, the nickel content varies from 49% to 57% (atomic % of Ni). The titanium composition in NiTi should be within 38–50% (atomic % of Ti) to acquire effective shape memory features. The characteristic physical, mechanical, and thermal transformation properties of NiTi are provided in Table 1 [16,52–62].

The NiTi-based SMAs with coil spring, wire, and foil structures are usually embedded into elastomeric materials to develop soft robotic actuators. When NiTi structures are assimilated into robotic mechanical joints [63–65], they can customarily provide large rotations with high torque because of their unique ability to withstand high strain (~200 to 1600%) and high force output [51,66]. Electrically driven tiny/micro-sized smart robotic actuators made with NiTi-based SMAs can perform natural sensitive biomimicking gesticulations like walking, jumping, climbing, whirling, and swimming. The advantages of using NiTi as one of the base materials is its corrosion resistibility and lightweight characteristics, especially when used in marine environments [67–69]. It is not surprising that SMAs ubiquitously reached technological maturity with promising industrial engineering applications in the mechatronics field amongst various smart materials. The unique phase transition

(martensitic–austenitic) behavior anticipated their actuation properties and allowed the development of significantly lightweight, compact, and soundless industrial actuators [70].

**Table 1.** Characteristic physical, mechanical, and thermal transformation properties of NiTi-based SMAs [16,52–62].

Physical Properties	
Density ( $\text{kg m}^{-3}$ )	6450–6500
Melting point ( $^{\circ}\text{C}$ )	ca. 1250–1310
Thermal conductivity of the austenite phase ( $\text{W m}^{-1} \text{K}^{-1}$ )	ca. 18
Thermal conductivity of the martensite phase ( $\text{W m}^{-1} \text{K}^{-1}$ )	ca. 9
Resistivity of the austenite phase ( $\mu\Omega \text{ cm}$ )	~100
Resistivity of the martensite phase ( $\mu\Omega \text{ cm}$ )	~70
Corrosion resistance	Excellent
Biocompatibility	Excellent
Magnetic susceptibility of the austenite phase ( $\text{emu g}^{-1}$ )	$3.7 \times 10^{-6}$
Magnetic susceptibility of the martensite phase ( $\text{emu g}^{-1}$ )	$2.4 \times 10^{-6}$
Magnetic permeability	<1.002
Specific heat ( $\text{cal g}^{-1} \text{ }^{\circ}\text{C}^{-1}$ )	0.2
Damping capacity (SDC %)	15–20
Heat capacity ( $\text{J kg}^{-1} \text{ K}^{-1}$ )	390
Mechanical properties	
Young's modulus of the austenite phase (GPa)	ca. 83
Young's modulus of the martensite phase (GPa)	ca. 23–41
Poisson's ratio	0.33
Elongation to fracture of the austenite phase	1–2%
Elongation to fracture of the martensite phase	Up to 60%
Plateau stress austenite phase (MPa)	200–650
Plateau stress martensite phase (MPa)	70–200
Yield strength austenite phase (MPa)	195–700
Yield strength martensite phase (MPa)	~70–140
Tensile strength (MPa)	895
Tensile strain (fully annealed form)	20–60
Normal working stress (GPa)	0.5–0.9
Ultimate tensile strength (GPa)	0.9
Fracture toughness ( $\text{MPa} \sqrt{\text{m}}$ )	895
Transformation temperature and strain properties	
Transformation temperature range ( $^{\circ}\text{C}$ )	−50 <sup>a</sup> –110
Transformation enthalpy ( $\text{kJ kg}^{-1} \text{ K}^{-1}$ )	0.47–0.62
Transformation strains: up to 1 cycle	Up to 8%
Transformation strains: up to 100 cycles	Up to 5%
Transformation strains: up to 100,000 cycles	Up to 3%
Transformation strains: above 100,000 cycles	ca. 2%
<sup>b</sup> Overall thermal hysteresis ( $^{\circ}\text{C}$ )	30–80
Hysteresis of martensite phase ( $^{\circ}\text{C}$ )	30–40
Hysteresis of R-phase ( $^{\circ}\text{C}$ )	2–5
Heat of transformation in martensite phase ( $\text{J mole}^{-1}$ )	295
Heat of transformation in R-phase ( $\text{J mole}^{-1}$ )	55
Latent heat of transformation ( $\text{cal g}^{-1}\text{-atom}$ )	40

<sup>a</sup> Low transformation temperature can be achieved by increasing nickel metal content; however, the nature of the material becomes highly brittle. <sup>b</sup> The hysteresis is calculated for complete load–unload cycles; however, the value is reduced for partial cycles.

The blended elemental powder metallurgy (BEPM) technique is one of the most common and cost-effective methods to produce intermetallic NiTi-based SMAs. As indicated from the binary phase diagram of NiTi [71], the eutectic composition transpires at 942 °C (at metallic compositions of 24.5 at. % of Ni, between the  $\beta$ -Ti and NiTi<sub>2</sub> intermetallic phase). It is believed that a stable Ni<sub>3</sub>Ti phase was evidently formed from the sequential decomposition of metastable phases (Ni<sub>4</sub>Ti<sub>3</sub> and Ni<sub>3</sub>Ti<sub>2</sub> phases), above the eutectic point for a longer duration [72].

The microstructure image displayed in Figure 8a represents the 80  $\mu\text{m}$  thick intermetallic phase of NiTi annealed at 900 °C for 100 h. As seen from Figure 8a, the gradual cooling process has generated two-phase regions in the NiTi phase. Hence, this unperturbed binary reactive diffusion process between Ni and Ti can be expressed as  $\text{NiTi} \rightarrow \text{Ni}_3\text{Ti} \rightarrow \text{NiTi}_2$ . Bertheville et al. [73] interpreted the needle-shaped particles observed in Figure 8b as martensitic NiTi, which can be easily discriminated from the austenitic phase using SEM and microstructure analysis and can be attributed to  $\text{Ni}_4\text{Ti}_3$  particles [74]. As speculated by the authors, at elevated temperatures, the  $\text{Ni}_4\text{Ti}_3$  phase gradually decomposed to the most stable and prominent  $\text{Ni}_3\text{Ti}$  phase via a precipitation sequence expressed as  $\text{Ni}_4\text{Ti}_3 \rightarrow \text{Ni}_3\text{Ti}_2 \rightarrow \text{Ni}_3\text{Ti}$ . Novák et al. [75] concluded that the self-propagating high-temperature synthesis (SHS) conditions can affect the microstructure of NiTi phases. Rapid heating (heating rate  $>300\text{ }^{\circ}\text{C min}^{-1}$ ), producing dominant NiTi and  $\text{Ti}_2\text{Ni}$  phases, can be perceived easily from microstructural analysis [75].

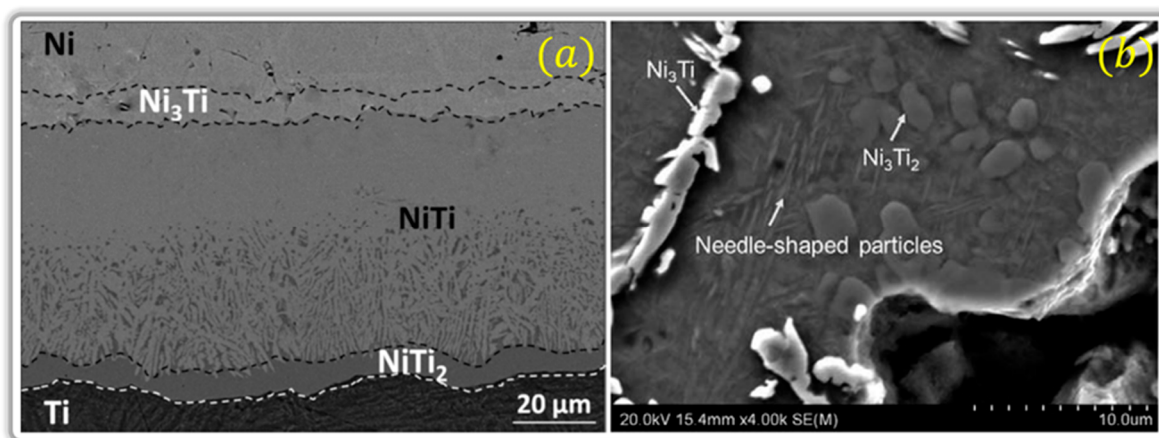


**Figure 8.** (a) The microstructure of interdiffusion zone in NiTi binary diffusion couple after annealing at 900 °C for 100 h. Adapted with permission from [71], Walter de Gruyter GmbH, Berlin/Boston, 2018. (b) SEM image of as-sintered samples prepared under processing conditions (pressing pressure: 400.0 MPa, sintering final temperature: 1050 °C, from ambient to 700 °C at heating rate  $10\text{ }^{\circ}\text{C min}^{-1}$ , 700–900 °C at heating rate  $2\text{ }^{\circ}\text{C min}^{-1}$ , 900–1050 °C at heating rate  $10\text{ }^{\circ}\text{C min}^{-1}$ , sintering holding time: 4 h). Adapted with permission from [74], Elsevier, 2018.

Aging of Ni-rich alloys at 400 °C can easily form noticeable lenticular  $\text{Ni}_4\text{Ti}_3$  precipitates. The stress fields due to the precipitates formed can result in the formation of an intermediate R-phase (the phase in between the austenite and martensite phases). This rhombohedral structure of the crystal phase (R-phase) generally disappears with heat treatment at higher temperatures [76,77]. Recent studies on 55 at. % of Ni in NiTi SMAs revealed that the composition exhibits transformation temperatures in the range of  $-10\text{ }^{\circ}\text{C}$  to  $60\text{ }^{\circ}\text{C}$ . This composition alloy is referred to as a chemically multi-phased alloy, so it exhibits low transformation strains and shows excellent corrosion resistance behavior as compared to stainless steel even in harsh saline environments [78]. Since these composition alloys show exceptional thermomechanical stability, they do not require cold working and can be hot formed into various complex shapes [79,80].

Nam et al. [81] preferentially replaced Ni in NiTi SMAs with copper (Cu) metal to obtain NiTiCu alloys. It was observed that the addition of Cu reduces the hysteresis of the shape memory response, and we can also notice a decrease in the transformation strain. In  $\text{Ni}_{40}\text{Ti}_{50}\text{Cu}_{10}$  (i.e., 10 at. % of Cu), the transformation hysteresis is much reduced to approximately 4%. In addition, the pseudoelastic hysteresis is less than 100 MPa, when compared to binary alloy ( $\text{Ni}_{50}\text{Ti}_{50}$ ). The addition of Cu greatly reduces the sensitivity of the martensitic phase start temperature to composition, influencing the material behavior associated with the change in phase transition [82]. Amongst diverse compositions of Cu,  $\leq 5\text{--}10$  at. % of Cu in NiTi is preeminent because it is associated with small hysteresis and

transformation, which is ideal for actuators. An at. % of Cu above 10% in NiTi influences the brittleness and the applications are constrained for actuator technologies [83].

The demand for high-temperature shape memory alloys (HTSMAs) has increased in the past few decades for aircraft engines and/or down-hole applications in oil-based industries [84]. The prime material criteria of HTSMAs is to have transformation temperatures  $> 100^{\circ}\text{C}$  and to have good actuating ability under high-temperature conditions [84]. The alloys produced by adding ternary elements, such as palladium (Pd), platinum (Pt), and gold (Au), to NiTi-based SMAs can widen the transformation temperature range to 100–800 °C [85,86]. Nicholson et al. [87] studied the thermomechanical behavior of NiTiPdPt HTSMA springs. The authors observed that the transformation strains are generally smaller compared to conventional NiTi alloys. The spring actuators made of Ni<sub>19.5</sub>Ti<sub>50.5</sub>Pd<sub>25</sub>Pt<sub>5</sub> (at. %) were subjected both monotonic axial loading and thermomechanical cycling. Larger strokes were obtained for the case of the rotationally unconstrained spring and maximum strokes were obtained at an intermediate load [87].

Due to the high cost associated with Pd, Pt, and Au, as alloying metals to NiTi, metals like hafnium (Hf) and zirconium (Zr) have been investigated to extend the commercial viability [88,89]. The composition Ni<sub>50.3</sub>Ti<sub>29.7</sub>Hf<sub>20</sub> (at.%) is the most widely studied because of its desirable actuation properties. The composition displays austenite finish temperatures ( $A_f$ ) of 150–200 °C (depending on slight alterations in the composition), and transformation strains above 3.5% in tension, 6% in torsion, and 2% in compression. In addition, it shows reasonable cyclic stability at high stresses, and high temperature superelasticity with more than 3% recoverable strain at  $> 200^{\circ}\text{C}$  [90]. The early works on niobium (Nb) as an alloying metal to NiTi for the composition Ni<sub>47</sub>Ti<sub>44</sub>Nb<sub>9</sub> (i.e., 9 at. % of Nb) showed that the insoluble globular precipitates of nearly pure Nb influence the deformation stress, equivalent to the detwinning stress of martensite [91]. The large thermal hysteresis of the composition is associated with the partitioning of the strain into a recoverable part (due to the NiTi phase) and an irrecoverable part (due to the Nb precipitates). The irregularities in the composition influence the mechanical properties and the material does not display complete recovery during deformation. Therefore, a Nb concentration around 3 at. % has shown promising shape memory effects [92,93].

Miniature NiTi spring actuators have conceivable applications in technological sectors. The performance of the actuator is highly dependent on the diameter of the coil ( $D$ ), the diameter of the wire ( $d$ ), and the number of active rings ( $n$ ) involved in the construction of spring. Many researchers have demonstrated and discussed thermodynamic models of NiTi springs for use as spring actuators [94–96]. The previously developed models do not explain the change in the spring's free length caused by the phase change phenomena in the NiTi microstructure. In the case of a complete martensite phase, the newly changed length  $X_{M_0}$  due to the elongation of the spring can be easily seen as well as its diminutive free length  $X_{A_0}$  in the complete austenite phase (see Figure 6). Additionally, the spring constant in the austenitic phase is about two to three times better than in its martensitic phase [60].

By adopting the techniques developed previously by Seok et al. [43] and Kim et al. [97], low spring index actuators were documented by Holschuh et al. [98]. The authors tuned the force-displacement characteristics of the spring structure by altering the geometry. In brief, winding a 305 μm NiTi wire (commercially known as 'Flexinnol' by Dynalloy Inc.) was carried out over a 635 μm stainless steel core, to achieve a spring index (C) ~3.08. The winding was accomplished as shown in Figure 9a, so as to attain a consistent pitch angle and tight packing density. After winding the wire at room temperature, the annealing of the wires was carried out at 450 °C for a short duration (~10 min) to fix the austenitic memory state of the spring before quenching in cold water. These annealing parameters are crucial [43], and decide the permanent plastic deformation after each actuation cycle of the spring (see Figure 9b). The annealing temperature decides various parameters of the spring actuator, specifically, (I) large annealing temperatures can affect the spring's ability to return to its original shape, (II) increasing the annealing temperature decreases

the detwinning force. The actuated NiTi coil in the twinned martensite state returns to its detwinned martensite state via martensite transformation. The external work should be necessary to perform this detwinning process and the extension of the coil results due to tensile force (pull force). This pull force is highly reliant on the annealing temperature, and is a mechanical characteristic of the actuators [43].

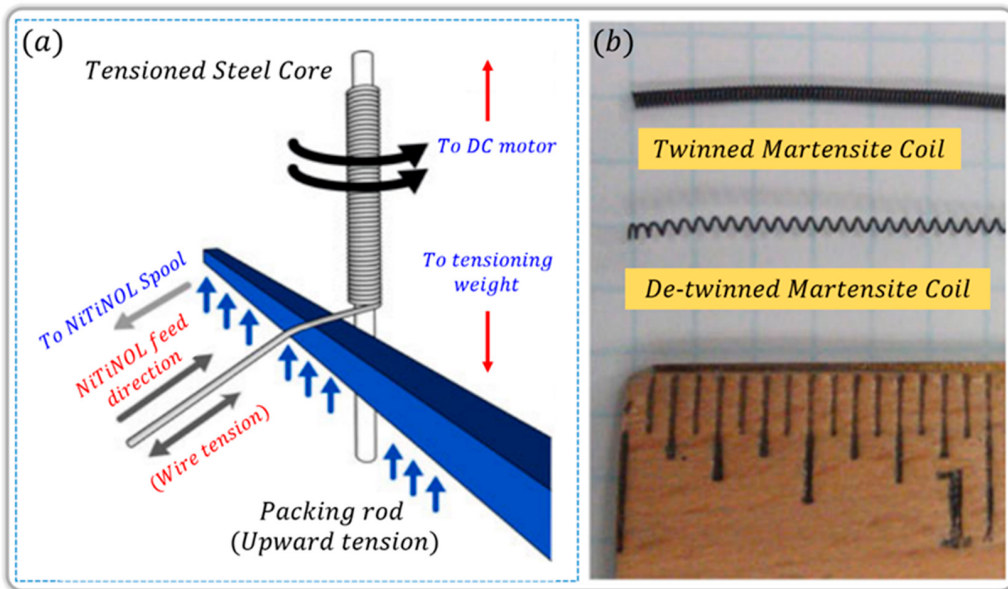


**Figure 9.** (a) Demonstration sketch of the winding technique developed by Seok et al. [43], Kim et al. [97], and Holschuh et al. [98], to achieve low spring index NiTi coil actuators. Adapted with permission from [43,97,98], IEEE, 2013, 2009, and 2015, respectively. (b) Pictograph representing finished twinned and detwinned NiTi coil spring actuators. Adapted with permission from [98], IEEE, 2015.

The as-prepared low spring index ( $C \sim 3.08$ ) NiTi coils by Holschuh et al. [98] demonstrated the increase in the actuation force upon applied voltage and extensional strain (up to 7.24 N). The authors firstly developed the compression tourniquet system embedded with these low index NiTi coils. During the activation cycle of the actuator, the system enables over a 70% increase in the applied pressure. This strategy can be effectively used to develop wearable smart fabrics, which dynamically tune their shape and size, for advanced applications ranging from healthcare sectors to designer smart shrink-wrapping spacesuits [99]. Tourniquet systems in association with sensors can expand the progressive impact in the event of any battlefield injury/bleeding or accidents, by impulsive compression of smart suits, and save lives.

Conceptual miniature robotic designs inspired by nature have advantageous technical implications in the human–robot interaction field [100,101]. Inspired by the locomotion patterns of an inchworm, Lobontiu et al. [102] and Lin et al. [103] have developed piezo-based and polymer-based tiny robots, respectively. Koh et al. [104] designed a sliding mini-robot, which bends its body in an omega ( $\Omega$ ) shape during crawling using NiTi coil springs. The authors named it ‘Omegabot’. To perform crawling locomotion, the total degrees of freedom were minimized by segmenting the robot with rigid links entailing four bar linkages and a steering mechanism, as shown in Figure 10a,b. The Z-shaped bending arises each time, generating one degree of freedom every time. The steering mechanism has three degrees of freedom (pitch, yaw, and roll) controlled by spherical six-bar linkages. The Omegabot prototype pictograph developed by Koh et al. [104] is presented in Figure 10c. These miniature robots can perform effortlessly in extremely harsh environments to execute emergency tasks [105,106].

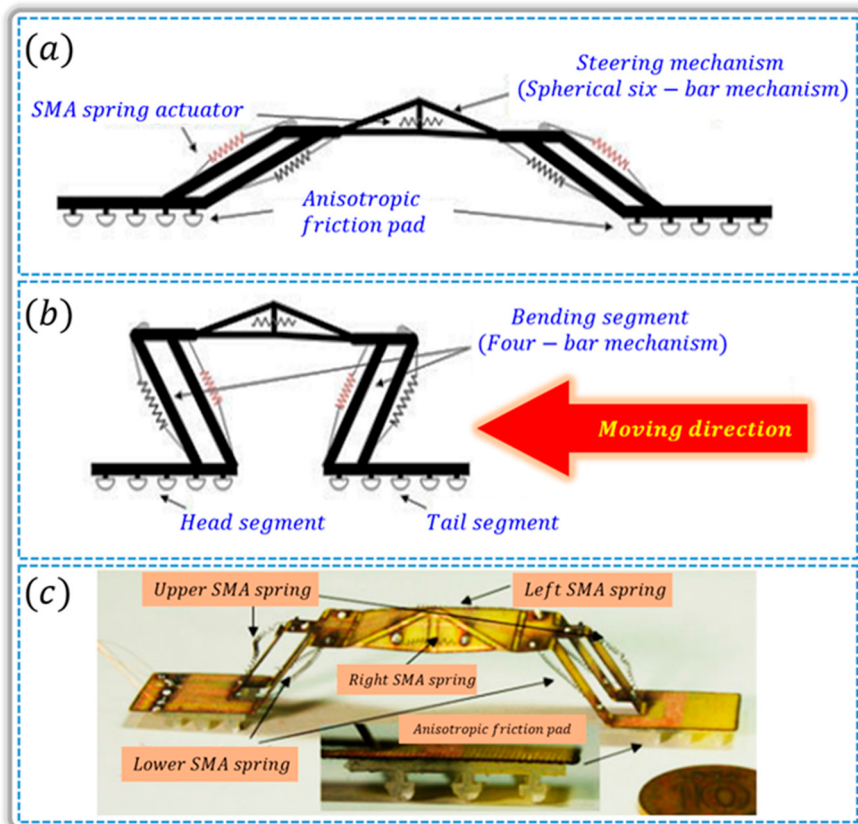


**Figure 10.** (a,b) Schematic design of the Omegabot developed by Koh et al. [104], (c) final prototype of an Omegabot. Note: red coils show the activated actuator. Adapted with permission from [104], IEEE, 2013.

High-cycle fatigue behavior of designed engineering materials is crucial for uninterrupted performances of actuators [107]. The pioneering works of Melton and Mercier [108] documented some fascinating trends. By varying  $A_f$  (austenite finish temperature) values between 10 and 110 °C, the binary compositions (NiTi) were studied at room temperature to obtain stimulating results. Interestingly, superelastic NiTi provides longer sustainability with superior fatigue limits than thermal martensite subjected to stress-control fatigue. The authors related this examination to the difference in plateau strength between austenite and martensite. The  $10^7$ -cycle stress fatigue limit is approximately 80% of the respective stress plateau (superelastic) or detwinning plateau (martensite) [108]. Recently, Jaureguizahar et al. [109] performed fatigue cycling of NiTi wire (diameter = 0.5 mm, 50.9 at. % Ni) using servo-hydraulic testing machines (MTS 810 and INSTRON 8800) equipped with respective environmental chambers. The results revealed that without pseudoelastic transformation, for the austenite and martensite phase, fatigue lives of  $10^7$  and  $9.33 \times 10^6$  were observed, respectively [109].

#### 4. Conclusions

This short technical note is a concise summary of the understanding of the properties of NiTi coil springs. Due to their unique thermo-mechanical performances, shape memory behavior, and high fatigue characteristics, NiTi-based smart and compact engineering structures have exceptional importance in actuator technologies. Their great elasticity under stress, corrosion resistivity, biocompatibility, and original shape remembering proficiency in thermal conditions have created excessive applications in various technological fields, including biomedical sectors. The NiTi coil springs can be attained by coiling straight-drawn NiTi wires; this can maximize the restorable linear strain limit up to 20%. The linear actuation stroke of NiTi wire actuators can be improved significantly by converting

them into coil spring structures. The specific inevitabilities and applicability of developed miniature robots activated by these coil spring structures could affect the final shape of the developed actuator. The inventive bioinspired designs and novel architecture of mini-robotic systems made of NiTi could comprehensively stimulate the commercial perspective [110,111].

**Author Contributions:** Conceptualization, data curation/formal analysis, writing original draft, G.S.; data curation/formal analysis, T.-H.K.; manuscript review, final editing and supervision, S.-Y.K. All authors have read and agreed to the published version of the manuscript.

**Funding:** This work was supported by the Priority Research Centers Program through the National Research Foundation of Korea (NRF) funded by the Ministry of Education (NRF-2018R1A6A1A03025526). This work was supported by a National Research Foundation of Korea (NRF) grant funded by the Ministry of Education (NRF-2020R1I1A3065371). This work was also supported by the Technology Innovation Program (10077367, Development of a film-type transparent/stretchable 3D touch sensor/haptic actuator combined module and advanced UI/UX) funded by the Ministry of Trade, Industry & Energy (MOTIE, Korea).

**Institutional Review Board Statement:** Not applicable.

**Informed Consent Statement:** Not applicable.

**Data Availability Statement:** Not applicable.

**Acknowledgments:** The authors acknowledge Cooperative Equipment Center at KoreaTech for formal discussions.

**Conflicts of Interest:** The authors declare no conflict of interest.

## References

1. Wikiwand. Mechatronics. Available online: <https://www.wikiwand.com/en/Mechatronics> (accessed on 16 April 2021).
2. Cetinkunt, S. *Mechatronics with Experiments*, 2nd ed.; John Wiley & Sons Ltd.: Chichester, UK, 2015; ISBN 9781118802465.
3. Moheimani, S.O.R. Mechatronics: 2021 and beyond. *Mechatronics* **2020**, *71*, 102446. [[CrossRef](#)]
4. Dixit, U.S.; Hazarika, M.; Davim, J.P. History of Mechatronics. In *A Brief History of Mechanical Engineering. Materials Forming, Machining and Tribology*; Springer: Cham, Switzerland, 2017; ISBN 978-3-319-42916-8. [[CrossRef](#)]
5. Liu, Y.-H. Medical Mechatronics for Healthcare. *J. Healthc. Eng.* **2018**, *2018*. [[CrossRef](#)]
6. Sharma, R.; Dhiman, B. Mechatronics Around the World—At a Glance. *J. Mechatron. Robot.* **2021**, *5*, 1–7. [[CrossRef](#)]
7. Pawlak, A.M. *Sensors and Actuators in Mechatronics: Design and Applications*, 1st ed.; CRC Press, Taylor & Francis Group: Boca Raton, FL, USA, 2007; ISBN 9780849390135.
8. Gorodetskiy, A.E. Smart Electromechanical Systems Modules. In *Smart Electromechanical Systems*; Gorodetskiy, A., Ed.; Studies in Systems, Decision and Control; Springer: Cham, Switzerland, 2016; ISBN 978-3-319-27547-5. [[CrossRef](#)]
9. Krishnan, R.V.; Bhaumik, S.K. Shape memory alloys: Properties and engineering applications. In *Smart Materials, Structures, and Systems*; Proc. SPIE 5062; International Society for Optics and Photonics: Bangalore, India, 2003. [[CrossRef](#)]
10. Zareie, S.; Issa, A.S.; Seethaler, R.J.; Zabihollah, A. Recent advances in the applications of shape memory alloys in civil infrastructures: A review. *Structures* **2020**, *27*, 1535–1550. [[CrossRef](#)]
11. Lobo, P.S.; Almeida, J.; Guerreiro, L. Shape Memory Alloys Behaviour: A Review. *Proc. Eng.* **2015**, *114*, 776–783. [[CrossRef](#)]
12. Crawford, M. Metal That Remembers Its Shape, The American Society of Mechanical Engineers. (1 July 2017). Available online: <https://www.asme.org/topics-resources/content/metal-that-remembers-its-shape> (accessed on 16 April 2021).
13. Wadood, A. Brief Overview on Nitinol as Biomaterial. *Adv. Mater. Sci. Eng.* **2016**, *2016*. [[CrossRef](#)]
14. Abubakar, R.A.; Wang, F.; Wang, L. A review on Nitinol shape memory alloy heat engines. *Smart Mater. Struct.* **2020**, *30*, 013001. [[CrossRef](#)]
15. Wang, Z.; Everaerts, J.; Salvati, E.; Korsunsky, A.M. Evolution of thermal and mechanical properties of Nitinol wire as a function of ageing treatment conditions. *J. Alloy. Compd.* **2020**, *819*, 153024. [[CrossRef](#)]
16. Huang, W. On the selection of shape memory alloys for actuators. *Mater. Des.* **2002**, *23*, 11–19. [[CrossRef](#)]
17. Kim, D.J.; Kim, H.A.; Chung, Y.-S.; Choi, E. Pullout resistance of straight NiTi shape memory alloy fibers in cement mortar after cold drawing and heat treatment. *Compos. Part B Eng.* **2014**, *67*, 588–594. [[CrossRef](#)]
18. Han, M.-W.; Rodrigue, H.; Cho, S.; Song, S.-H.; Wang, W.; Chu, W.-S.; Ahn, S.-H. Woven type smart soft composite for soft morphing car spoiler. *Compos. Part B Eng.* **2016**, *86*, 285–298. [[CrossRef](#)]
19. Swensen, J.P.; Doller, A.M. Optimization of Parallel Spring Antagonists for Nitinol Shape Memory Alloy Actuators. In Proceedings of the IEEE International Conference on Robotics and Automation (ICRA), Hong Kong, China, 31 May–7 June 2014. [[CrossRef](#)]

20. Stachiv, I.; Alarcon, E.; Lamac, M. Shape Memory Alloys and Polymers for MEMS/NEMS Applications: Review on Recent Findings and Challenges in Design, Preparation, and Characterization. *Metals* **2021**, *11*, 415. [[CrossRef](#)]
21. Liu, Y.; Liu, Y.; Humbeeck, V.J. Luders-like deformation associated with martensite reorientation in NiTi. *Scr. Mater.* **1998**, *39*, 665213. [[CrossRef](#)]
22. Alkan, S.; Sehitoglu, H. Prediction of transformation stresses in NiTi shape memory alloy. *Acta Mater.* **2019**, *175*, 182–195. [[CrossRef](#)]
23. Polatidis, E.; Šmíd, M.; Kuběna, I.; Hsu, W.-N.; Laplanche, G.; Swygenhoven, H.V. Deformation mechanisms in a superelastic NiTi alloy: An in-situ high resolution digital image correlation study. *Mater. Des.* **2020**, *191*, 108622. [[CrossRef](#)]
24. Gall, K.A. The effect of Stress State and Precipitation on Stress-Induced Martensitic Transformations in Polycrystalline and Single Crystal Shape Memory Alloys: Experiments and Micro-Mechanical Modeling. Ph.D. Thesis, University of Illinois, Urbana, IL, USA, 1998. Available online: <https://www.proquest.com/docview/304447772?pq-origsite=gscholar&fromopenview=true> (accessed on 16 July 2021).
25. Dynalloy, Inc. Flexinol® Actuator Wire Technical and Design Data. Available online: [https://www.dynalloy.com/tech\\_data\\_wire.php](https://www.dynalloy.com/tech_data_wire.php) (accessed on 16 April 2021).
26. Kheirikhah, M.M.; Rabiee, S.; Edalat, M.E. A Review of Shape Memory Alloy Actuators in Robotics. In *Lecture Notes in Computer Science*; Ruiz-del-Solar, J., Chown, E., Plöger, P.G., Eds.; RoboCup 2010: Robot Soccer World Cup XIV. RoboCup 2010; Springer: Berlin/Heidelberg, Germany, 2011; Volume 6556. [[CrossRef](#)]
27. Kapoor, D. Nitinol for Medical Applications: A Brief Introduction to the Properties and Processing of Nickel Titanium Shape Memory Alloys and their Use in Stents. *Johns. Matthey Technol. Rev.* **2017**, *61*, 66–76. [[CrossRef](#)]
28. Otsuka, K.; Ren, X. Physical metallurgy of Ti–Ni-based shape memory alloys. *Prog. Mater. Sci.* **2005**, *50*, 511–678. [[CrossRef](#)]
29. Contardo, L.; Guenin, G. Training and two-way memory effect in Cu-Zn-Al alloy. *Acta Metall. Mater.* **1990**, *38*, 1267–1272. [[CrossRef](#)]
30. Chekotu, J.C.C.; Groarke, R.; O'Toole, K.; Brabazon, D. Advances in Selective Laser Melting of Nitinol Shape Memory Alloy Part Production. *Materials* **2019**, *12*, 809. [[CrossRef](#)] [[PubMed](#)]
31. Saedi, S. Shape Memory Behavior of Dense and Porous NiTi Alloys Fabricated by Selective Laser Melting. Ph.D. Thesis, University of Kentucky, Lexington, KY, USA, 2017. Available online: [https://uknowledge.uky.edu/me\\_etds/90/](https://uknowledge.uky.edu/me_etds/90/) (accessed on 19 April 2021).
32. Huang, X.; Ackland, G.J.; Rabe, K.M. Crystal structures and shape-memory behaviour of NiTi. *Nat. Mater.* **2003**, *2*, 307–311. [[CrossRef](#)] [[PubMed](#)]
33. Parlinski, K.; Parlinska-Wojtan, M. Lattice dynamics of NiTi austenite, martensite and R-phase. *Phys. Rev. B* **2002**, *66*, 064307. [[CrossRef](#)]
34. Proffit, W.; Fields, H. *Contemporary Orthodontics*, 5th ed.; Elsevier: St. Louis, MO, USA, 2012; pp. 359–394. ISBN 9780323291521.
35. Lagoudas, D.C. *Shape Memory Alloys, Modeling and Engineering Applications*; Springer: Austin, TX, USA, 2008; ISBN 9780387476858.
36. Bucsek, A.N.; Paranjape, H.M.; Stebner, A.P. Myths and Truths of Nitinol Mechanics: Elasticity and Tension–Compression Asymmetry. *Shap. Mem. Superelasticity* **2016**, *2*, 264–271. [[CrossRef](#)]
37. Yuan, H.; Fauroux, J.-C.; Chapelle, F. A review of rotary actuators based on shape memory alloys. *J. Intell. Mater. Syst. Struct.* **2017**, *28*, 1863–1885. [[CrossRef](#)]
38. Jani, J.M.; Leary, M.; Subic, A. Designing shape memory alloy linear actuators: A review. *J. Intell. Mater. Syst. Struct.* **2016**, *28*, 1699–1718. [[CrossRef](#)]
39. Song, G. Design and control of a Nitinol wire actuated rotary servo. *Smart Mater. Struct.* **2007**, *16*, 1796. [[CrossRef](#)]
40. Jani, J.M. Design Optimisation of Shape Memory Alloy Linear Actuator Applications. Ph.D. Thesis, RMIT University, Melbourne, Australia, 2016. Available online: <https://core.ac.uk/download/pdf/43495833.pdf> (accessed on 19 April 2021).
41. Kónya, A.; Maxin, M.; Wright, K.C. New Embolization Coil Containing a Nitinol Wire Core: Preliminary In Vitro and In Vivo Experiences. *J. Vasc. Interv. Radiol.* **2001**, *12*, 869–877. [[CrossRef](#)]
42. Koh, J.-S. Design of Shape Memory Alloy Coil Spring Actuator for Improving Performance in Cyclic Actuation. *Materials* **2018**, *11*, 2324. [[CrossRef](#)]
43. Seok, S.; Onal, C.D.; Cho, K.-J.; Wood, R.J.; Rus, D.; Kim, S. Meshworm: A Peristaltic Soft Robot with Antagonistic Nickel Titanium Coil Actuators. *IEEE/ASME Trans. Mechatron.* **2013**, *18*, 1485–1497. [[CrossRef](#)]
44. Tan, P.S.; Farid, A.A.; Karimzadeh, A.; Koloor, S.S.R.; Petrù, M. Investigation on the Curvature Correction Factor of Extension Spring. *Materials* **2020**, *13*, 4199. [[CrossRef](#)]
45. Liu, Y. Detwinning process and its anisotropy in shape memory alloys. *Proc. SPIE Smart Mater.* **2001**, *4234*, 82–93. [[CrossRef](#)]
46. Liu, Y. On the Detwinning Mechanism in Shape Memory Alloys. In Proceedings of the IUTAM Symposium on Mechanics of Martensitic Phase Transformation in Solids. Solid Mechanics and Its Applications, Hong Kong, China, 11–15 June 2001; Sun, Q.P., Ed.; Springer: Dordrecht, The Netherlands, 2002; Volume 101. ISBN 978-94-017-0069-6. [[CrossRef](#)]
47. Mehrpouya, M.; Bidsorkhi, H.C. MEMS Applications of NiTi Based Shape Memory Alloys: A Review. *Micro Nanosyst.* **2016**, *8*, 79–91. [[CrossRef](#)]
48. Costanza, G.; Tata, M.E. Shape Memory Alloys for Aerospace, Recent Developments, and New Applications: A Short Review. *Materials* **2020**, *13*, 1856. [[CrossRef](#)]
49. Soother, D.K.; Daudpoto, J.; Chowdhry, B.S. Challenges for practical applications of shape memory alloy actuators. *Mater. Res. Express* **2020**, *7*, 073001. [[CrossRef](#)]

50. Huang, X.; Ford, M.; Patterson, Z.J.; Zarepoor, M.; Pan, C.; Majidi, C. Shape memory materials for electrically-powered soft machines. *J. Mater. Chem. B* **2020**, *8*, 4539–4551. [CrossRef] [PubMed]
51. Rich, S.I.; Wood, R.J.; Majidi, C. Untethered soft robotics. *Nat. Electron.* **2018**, *1*, 102–112. [CrossRef]
52. Jani, J.M.; Leary, M.; Subic, A.; Gibson, M.A. A review of shape memory alloy research, applications and opportunities. *Mater. Des.* **2014**, *56*, 1078–1113. [CrossRef]
53. Barbarino, S.; Saavedra Flores, E.L.; Ajaj, R.M.; Dayyani, I.; Friswell, M.I. A review on shape memory alloys with applications to morphing aircraft. *Smart Mater. Struct.* **2014**, *23*, 063001. [CrossRef]
54. Johnson Matthey Inc. Available online: <http://www.jmmedical.com/> (accessed on 20 April 2021).
55. Kumar, G. Modeling and Design of one Dimensional Shape Memory Alloy Actuators. Master’s Thesis, The Ohio State University, Columbus, OH, USA, 2000. Available online: [https://etd.ohiolink.edu/apexprod/rws\\_olink/r/1501/10?p10\\_etd\\_subid=63836&clear=10](https://etd.ohiolink.edu/apexprod/rws_olink/r/1501/10?p10_etd_subid=63836&clear=10) (accessed on 20 April 2021).
56. Andani, M.T. Constitutive Modeling of Superelastic Shape Memory Alloys Considering Rate Dependent Non-Mises Tension-torsion Behavior. Master’s Thesis, The University of Toledo, Toledo, OH, USA, 2013. Available online: [https://etd.ohiolink.edu/apexprod/rws\\_etd/send\\_file/send?accession=toledo1371577037&disposition=inline](https://etd.ohiolink.edu/apexprod/rws_etd/send_file/send?accession=toledo1371577037&disposition=inline) (accessed on 20 April 2021).
57. Fugazza, D. Use of Shape-Memory Alloy Devices in Earthquake Engineering: Mechanical Properties, Advanced Constitutive Modelling and Structural Applications. Ph.D. Thesis, University of Pavia, Pavia, Italy, 2005. Available online: <https://citeseerx.ist.psu.edu/viewdoc/download?doi=10.1.1.623.2545&rep=rep1&type=pdf> (accessed on 20 April 2021).
58. SMA Group. Available online: <http://smagroup.blogspot.com/2009/04/shape-memory-alloy-sma-also-known-as.html> (accessed on 20 April 2021).
59. Srinivasan, A.V.; McFarland, D.M. *Smart Structures: Analysis and Design*; Cambridge University Press: Cambridge, UK, 2001; ISBN 0521650267.
60. Otsuka, K.; Wayman, C.M. *Shape Memory Materials*; Cambridge University Press: Cambridge, UK, 1999; ISBN 9780521663847.
61. LExcellent, C. *Shape-Memory Alloys Handbook*; Wiley-ISTE Publisher Ltd.: London, UK, 2013; ISBN 9781848214347.
62. Tanzi, M.-C.; Fare, S.; Candiani, G. Part II Biomaterials and Biocompatibility, Chapter 4. Biomaterials and Applications. In *Foundations of Biomaterials Engineering*, 1st ed.; Academic Press—Elsevier: Cambridge, MA, USA, 2019.
63. Taylor, A.J.; Slutsky, T.; Feuerman, L.; Ren, H.; Tokuda, J.; Nilsson, K.; Tse, Z.T.H. MR-Conditional SMA-Based Origami Joint. *IEEE/ASME Trans. Mechatronics* **2019**, *24*, 883–888. [CrossRef]
64. Cheng, S.S.; Kim, Y.; Desai, J.P. Modeling and characterization of shape memory alloy springs with water cooling strategy in a neurosurgical robot. *J. Intell. Mater. Syst. Struct.* **2017**, *28*, 2167–2183. [CrossRef]
65. Yang, H.; Xu, M.; Li, W.; Zhang, S. Design and Implementation of a Soft Robotic Arm Driven by SMA Coils. *IEEE Trans. Ind. Electron.* **2019**, *66*, 6108–6116. [CrossRef]
66. An, S.M.; Ryu, J.; Cho, M.; Cho, K.J. Engineering design framework for a shape memory alloy coil spring actuator using a static two-state model. *Smart Mater. Struct.* **2012**, *21*, 055009. [CrossRef]
67. Sreekumar, M.; Nagarajan, T.; Singaperumal, M.; Zoppi, M.; Molfino, R.M. Critical review of current trends in shape memory alloy actuators for intelligent robots. *Ind. Robot* **2007**, *34*, 285–294. [CrossRef]
68. Cuéllar, W.H.C. BR3: A Biologically Inspired Fish-Like Robot Actuated by SMA-Based Artificial Muscles. Ph.D. Thesis, Universidad Politécnica de Madrid, Madrid, Spain, 2015. Available online: [http://oa.upm.es/36254/1/WILLIAM\\_HERNAN\\_CORAL\\_CUELLAR.pdf](http://oa.upm.es/36254/1/WILLIAM_HERNAN_CORAL_CUELLAR.pdf) (accessed on 20 April 2021).
69. Ulloa, C.C.; Terrile, S.; Barrientos, A. Soft Underwater Robot Actuated by Shape-Memory Alloys “JellyRobcib” for Path Tracking through Fuzzy Visual Control. *Appl. Sci.* **2020**, *10*, 7160. [CrossRef]
70. Spaggiari, A.; Castagnetti, D.; Golinelli, N.; Dragoni, E.; Mammano, G.S. Smart materials: Properties, design and mechatronic applications. *Proc. Inst. Mech. Eng. Part L J. Mater. Des. Appl.* **2019**, *233*, 734–762. [CrossRef]
71. Wierzba, B.; Nowak, W.J.; Serafin, N. The Interface Reaction between Titanium and Iron-Nickel alloys. *High Temp. Mater. Proc.* **2018**, *37*. [CrossRef]
72. Hornbuckle, B.C.; Xiao, X.Y.; Noebe, R.D.; Martens, R.; Weaver, M.L.; Thompson, G.B. Hardening behavior and phase decomposition in very Ni-rich Nitinol alloys. *Mater. Sci. Eng.* **2015**, *639*, 336–344. [CrossRef]
73. Bertheville, B.; Neudenberger, M.; Bidaux, J.-E. Powder sintering and shape-memory behaviour of NiTi compacts synthesized from Ni and TiH<sub>2</sub>. *Mater. Sci. Eng.* **2004**, *384*, 143–150. [CrossRef]
74. Khanlari, K.; Ramezani, M.; Kelly, P.; Cao, P.; Neitzert, T. Mechanical and microstructural characteristics of as-sintered and solutionized porous 60NiTi. *Intermetallics* **2018**, *100*, 32–43. [CrossRef]
75. Novák, P.; Mejzlíková, L.; Michalcová, A.; Čapek, J.; Beran, P. Effect of SHS conditions on microstructure of NiTi shape memory alloy. *Intermetallics* **2013**, *42*, 85–91. [CrossRef]
76. Buehler, W.J.; Wiley, R.C. Nickel-Base Alloys. U.S. Patent US3174851A, 23 March 1965.
77. Miyazaki, S.; Otsuka, K. Deformation and transformation behavior associated with the r-phase in Ti-Ni alloys. *Metall. Trans. A* **1986**, *17*, 53–63. [CrossRef]
78. Dębska, A.; Gwoździewicz, P.; Seruga, A.; Balandraud, X.; Destrebecq, J.-F. The Application of Ni-Ti SMA Wires in the External Prestressing of Concrete Hollow Cylinders. *Materials* **2021**, *14*, 1354. [CrossRef]

79. Clingman, D.J.; Calkins, F.T.; Smith, J.P. Thermomechanical properties of Ni60%weightTi40%weight. In *Proceedings of the SPIE, Smart Structures and Materials: Active Materials: Behavior and Mechanics*; International Society for Optics and Photonics: Bellingham, WA, USA, 2003; Volume 5053, pp. 219–229. [[CrossRef](#)]
80. Mabe, J.; Ruggeri, R.; Calkins, F.T. Characterization of nickel-rich nitinol alloys for actuator development. In Proceedings of the International Conference on Shape Memory and Superelasticity Technologies, Pacific Grove, CA, USA, 7–11 May 2006. [[CrossRef](#)]
81. Nam, T.H.; Saburi, T.; Shimizu, K. Cu-Content Dependence of Shape memory Characteristics in Ti-Ni-Cu Alloys. *Mater. Trans. JIM* **1990**, *31*, 959–967. [[CrossRef](#)]
82. Liu, Y. Mechanical and thermomechanical properties of a  $Ti_{0.50}Ni_{0.25}Cu_{0.25}$  melt spun ribbon. *Mater. Sci. Eng. A* **2003**, *354*, 286–291. [[CrossRef](#)]
83. Xie, Z.L.; Van Humbeeck, J.; Liu, Y.; Delaey, L. TEM study of  $Ti_{50}Ni_{25}Cu_{25}$  melt spun ribbons. *Scripta Materialia* **1997**, *37*, 363–371. [[CrossRef](#)]
84. Ma, J.; Karaman, I.; Noebe, R.D. High temperature shape memory alloys. *Int. Mater. Rev.* **2013**, *55*, 257–315. [[CrossRef](#)]
85. Benafan, O.; Garg, A.; Noebe, R.D.; Bigelow, G.S.; Padula, S.A., II; Gaydosh, D.J.; Vaidyanathan, R.; Clausen, B.; Vogel, S. Thermomechanical behavior and microstructural evolution of a Ni-rich  $Ni_{24.3}Ti_{49.7}Pd_{26}$  high temperature shape memory alloy. *J. Alloy. Compd.* **2015**, *643*, 275–289. [[CrossRef](#)]
86. Yamabe-Mitarai, Y.; Arockiakumar, R.; Wadood, A.; Suresh, K.S.; Kitashima, T.; Hara, T.; Shimojo, M.; Tasaki, W.; Takahashi, M.; Takahashi, S.; et al. Ti(Pt, Pd, Au) based High Temperature Shape Memory Alloys. *Mater. Today Proc.* **2015**, *2*, S517–S522. [[CrossRef](#)]
87. Nicholson, D.E.; Padula, S.A., II; Noebe, R.D.; Benafan, O.; Vaidyanathan, R. Thermomechanical behavior of NiTiPdPt high temperature shape memory alloy springs. *Smart Mater. Struct.* **2014**, *23*, 125009. [[CrossRef](#)]
88. Oliveira, J.P.; Schell, N.; Zhou, N.; Wood, L.; Benafan, O. Laser welding of precipitation strengthened Ni-rich NiTiHf high temperature shape memory alloys: Microstructure and mechanical properties. *Mater. Des.* **2019**, *162*, 229–234. [[CrossRef](#)]
89. Ramos, A.P.; de Castro, W.B.; Costa, J.D.; de Santana, R.A. Influence of Zirconium Percentage on Microhardness and Corrosion Resistance of  $Ti_{50}Ni_{50-x}Zr_x$  Shape Memory Alloys. *Mater. Res.* **2019**, *22*, e20180604. [[CrossRef](#)]
90. Bigelow, G.S.; Benafan, O.; Garg, A.; Noebe, R.D. Effect of Hf/Zr Ratio on Shape Memory Properties of High Temperature Ni<sub>50.3</sub>Ti<sub>29.7</sub>(Hf,Zr)<sub>20</sub> Alloys. *Scr. Mater.* **2021**, *194*, 113623. [[CrossRef](#)]
91. Zhang, C.S.; Zhao, L.C.; Duerig, T.W.; Wayman, C.M. Effects of deformation on the transformation hysteresis and shape memory effect in a  $Ni_{47}Ti_{44}Nb_9$  alloy. *Scr. Metall. Mater.* **1990**, *24*, 1807–1812. [[CrossRef](#)]
92. Zhao, L.C.; Duerig, T.W.; Justi, S.; Melton, K.N.; Proft, J.L.; Yu, W.; Wayman, C.M. The study of niobium-rich precipitates in a Ni-Ti-Nb shape memory alloy. *Scr. Metall. Mater.* **1990**, *24*, 221–226. [[CrossRef](#)]
93. He, X.M.; Rong, L.J.; Yan, D.S.; Li, Y.Y. TiNiNb wide hysteresis shape memory alloy with low niobium content. *Mater. Sci. Eng. A* **2004**, *371*, 193–197. [[CrossRef](#)]
94. Dong, Y.; Boming, Z.; Jun, L. A changeable aerofoil actuated by shape memory alloy springs. *Mater. Sci. Eng. A* **2008**, *485*, 243–250. [[CrossRef](#)]
95. Kim, B.; Lee, M.G.; Lee, Y.P.; Kim, Y.; Lee, G. An earthworm-like micro robot using shape memory alloy actuator. *Sens. Actuators A Phys.* **2006**, *125*, 429–437. [[CrossRef](#)]
96. Lee, H.J.; Lee, J.J. Evaluation of the characteristics of a shape memory alloy spring actuator. *Smart Mater. Struct.* **2000**, *9*, 817. [[CrossRef](#)]
97. Kim, S.; Hawkes, E.; Cho, K.; Jolda, M.; Foley, J.; Wood, R. Micro artificial muscle fiber using NiTi spring for soft robotics. In Proceedings of the 2009 IEEE/RSJ International Conference on Intelligent Robots and Systems, St. Louis, MO, USA, 10–15 October 2009; pp. 2228–2234. [[CrossRef](#)]
98. Holschuh, B.; Obropta, E.; Newman, D. Low Spring Index NiTi Coil Actuators for Use in Active Compression Garments. *IEEE/ASME Trans. Mechatron.* **2015**, *20*, 1264–1277. [[CrossRef](#)]
99. Chu, J. Shrink-wrapping spacesuits, spacesuits of the future may resemble a streamlined second skin. *MIT News* September-2014. Available online: <https://news.mit.edu/2014/second-skin-spacesuits-0918> (accessed on 22 April 2021).
100. Shimoga, G.; Choi, D.-S.; Kim, S.-Y. Bio-Inspired Soft Robotics: Tunable Photo-Actuation Behavior of Azo Chromophore Containing Liquid Crystalline Elastomers. *Appl. Sci.* **2021**, *11*, 1233. [[CrossRef](#)]
101. Clabaugh, C.; Matarić, M. Robots for the people, by the people: Personalizing human-machine interaction. *Sci. Robot.* **2018**, *3*, eaat7451. [[CrossRef](#)]
102. Lobontiu, N.; Goldfarb, M.; Garcia, E. A piezoelectric-driven inchworm locomotion device. *Mech. Mach. Theory* **2001**, *36*, 425–443. [[CrossRef](#)]
103. Lin, H.; Leisk, G.; Trimmer, B. GoQBot: A caterpillar-inspired softbodied rolling robot. *Bioinspiration Biomim.* **2011**, *6*, 026007. [[CrossRef](#)]
104. Koh, J.-S.; Cho, K.-J. Omega-Shaped Inchworm-Inspired Crawling Robot with Large-Index-and-Pitch (LIP) SMA Spring Actuators. *IEEE/ASME Transactions Mechatron.* **2013**, *18*, 419–429. [[CrossRef](#)]
105. Wong, C.; Yang, E.; Yan, X.-T.; Gu, D. Autonomous robots for harsh environments: A holistic overview of current solutions and ongoing challenges. *Syst. Sci. Control Eng.* **2018**, *6*, 213–219. [[CrossRef](#)]
106. Tsitsimpelis, I.; Taylor, C.J.; Lennox, B.; Joyce, M.J. A review of ground-based robotic systems for the characterization of nuclear environments. *Prog. Nucl. Energy* **2019**, *111*, 109–124. [[CrossRef](#)]

107. Wheeler, R.W. Actuation Fatigue Characterization Methods and Lifetime Predictions of Shape Memory Alloy Actuators. Ph.D. Thesis, Texas A&M University, College Station, TX, USA, 2017. Available online: <https://core.ac.uk/download/pdf/147255901.pdf> (accessed on 8 June 2021).
108. Melton, K.N.; Mercier, O. Fatigue of NiTi thermoelastic martensites. *Acta Metall.* **1979**, *27*, 137–144. [[CrossRef](#)]
109. Jaureguizahar, S.M.; Chapetti, M.D.; Yawny, A.A. Fatigue of NiTi shape memory wires. *Procedia Struct. Integr.* **2016**, *2*, 1427–1434. [[CrossRef](#)]
110. Nespoli, A.; Bessegini, S.; Pittaccio, S.; Villa, E.; Viscuso, S. The high potential of shape memory alloys in developing miniature mechanical devices: A review on shape memory alloy mini-actuators. *Sens. Actuators A Phys.* **2010**, *158*, 149–160. [[CrossRef](#)]
111. Zainal, M.A.; Sahlani, S.; Ali, M.S.M. Micromachined Shape-Memory-Alloy Microactuators and Their Application in Biomedical Devices. *Micromachines* **2015**, *6*, 879–901. [[CrossRef](#)]